THE ASTRONOMICAL JOURNAL, 117:3041–3053, 1999 June

ORBITAL EVOLUTION OF PLANETS EMBEDDED IN A PLANETESIMAL DISK

JOSEPH M. HAHN AND RENU MALHOTRA
Lunar and Planetary Institute, 3600 Bay Area Boulevard, Houston, TX 77058-1113; hahn@lpi.jsc.nasa.gov, renu@lpi.jsc.nasa.gov
Received 1998 December 29; accepted 1999 February 16

ABSTRACT

The existence of the Oort comet cloud, the Kuiper belt, and plausible inefficiencies in planetary core formation all suggest that there was once a residual planetesimal disk of mass $\sim$10–100 $M_\oplus$ in the vicinity of the giant planets following their formation. Since removal of this disk requires an exchange of orbital energy and angular momentum with the planets, significant planetary migration can ensue. The planet migration phenomenon is examined numerically by evolving the orbits of the giant planets while they are embedded in a planetesimal disk having a mass of $M_D = 10$–$200\ M_\oplus$. We find that Saturn, Uranus, and Neptune evolve radially outward as they scatter the planetesimals, while Jupiter's orbit shrinks as it ejects mass. Higher mass disks result in more rapid and extensive planet migration. If orbital expansion and resonance trapping by Neptune are invoked to explain the eccentricities of Pluto and its cohort of Kuiper belt objects at Neptune's 3:2 mean motion resonance, then our simulations suggest that a disk mass of order $M_D \sim 50\ M_\oplus$ is required to expand Neptune's orbit by $\Delta a \sim 7$ AU, in order to pump up Plutino eccentricities to $e \sim 0.3$. Such planet migration implies that the solar system was more compact in the past, with the initial Jupiter-Neptune separation having been smaller by about 30%.

We discuss the fate of the remnants of the primordial planetesimal disk. We point out that most of the planetesimal disk beyond Neptune's 2:1 resonance should reside in nearly circular, low-inclination orbits, unless there are (or were) additional, unseen, distant perturbers. The planetesimal disk is also the source of the Oort cloud of comets. Using the results of our simulations together with a simple treatment of Oort cloud dynamics, we estimate that $\sim$12 $M_\oplus$ of disk material was initially deposited in the Oort cloud, of which $\sim$4 $M_\oplus$ will persist over the age of the solar system. The majority of these comets originated from the Saturn-Neptune region of the solar nebula.

Key words: Kuiper belt, Oort cloud — solar system: formation

1. INTRODUCTION

It is generally accepted that a final distinct stage in the formation of our planetary system consisted of the clearing of a residual planetesimal population by the gravitational perturbations of fully formed giant planets. The formation of the Oort cloud, which is a spherical swarm of comets orbiting the Sun at distances of $\sim 10^3$–10^5 AU, is thought to be a product of this stage of solar system formation. Mass estimates for the Oort cloud are in the range $\sim$10 to 100 $M_\oplus$ (Weissman 1996). Another remnant of the planetesimal disk is the recently discovered population of the Kuiper belt objects (KBOs) that orbit beyond Neptune. Although the mass of the observable portion of the Kuiper belt is only $\sim 0.26\ M_\oplus$ (Jewitt, Luu, & Trujillo 1998), planetesimal accretion models require an initial mass that is of order $\sim 35\ M_\oplus$ for the assembly of Pluto and the $R \sim 100$ km–sized KBOs in the 30–50 AU zone (Stern & Colwell 1997; Kenyon & Luu 1998). Noting also that the solid cores of the giant planets are of order $\sim 10\ M_\oplus$, and that core formation is not likely to have been 100% efficient, it is quite plausible that there was still a residual planetesimal disk of mass $\sim$10–100 $M_\oplus$ in the vicinity of the giant planets after they formed. The eventual removal of this mass via gravitational scattering by the giant planets could have caused significant evolution of the planetary orbits, such that the presently observed orbital configuration of the Jovian planets is considerably altered from that obtained soon after their formation.

Not only is an early epoch of planet migration plausible based upon formation considerations, but recent advances in our knowledge of the outer solar system provide new motivation for studying this process. The determination of reasonably reliable orbits for several dozen KBOs has revealed that their distribution is quite nonuniform: there is a near-complete dearth of KBOs having semimajor axes a interior to Neptune's 3:2 mean motion resonance at 39.4 AU, and there is a prominent concentration of objects at the 3:2 resonance with moderately high eccentricities $e \sim 0.1$–0.35 (Jewitt et al. 1998). Several other KBOs orbit at the 4:3, 5:3, and 2:1 resonances, all with moderately high eccentricities. There is also a nonresonant KBO population beyond the 3:2 resonance, which extends out to 47 AU; these objects exist in more circular orbits with $e \lesssim 0.1$. This peculiar orbital distribution supports the hypothesis that Neptune's orbit migrated radially outward, sweeping the primordial Kuiper belt with that planet's mean motion resonances and capturing Pluto, as well as a cohort of KBOs, at those resonances (Malhotra 1993, 1995). Both the semimajor axes and the eccentricities of captured bodies would have grown concurrently with the planet's orbital expansion. The inclinations of KBOs can also become excited when a vertical secular resonance sweeps past (Malhotra 1998). Analysis of the resonance-sweeping mechanism shows that if planet migration were responsible for the eccentric and inclined orbits of Pluto and the other KBOs at the 3:2 resonance, then Neptune's orbit must have expanded by 5 AU $\lesssim \Delta a \lesssim$ 10 AU on a timescale of order $\tau_m \sim 10^7$ yr or longer (Malhotra 1993, 1998). Malhotra (1999) estimated that the gravitational clearing of a residual planetesimal disk having a mass of about 35 $M_\oplus$ distributed

in the vicinity of Uranus and Neptune would expand Neptune's orbit by $\Delta a \sim 5$ AU. The planet migration/resonance-sweeping hypothesis not only accounts for the abundance of eccentric, inclined KBOs locked in orbital resonance with Neptune, it also accounts for the lack of low-eccentricity orbits in the 3:2 resonance and the depleted region interior to the 3:2, as well as the excited $e \sim 0.1$ state of the nonresonant KBOs. It is thus possible that the characteristics of the orbital migration history of Neptune (and, by extension, the other giant planets) is preserved in the details of the KBO orbital distribution.

Orbital migration was first noted in the giant-planet accretion models of Fernández & Ip (1984), which showed that the orbits of a growing proto-Uranus and proto-Neptune could shift by $\sim$5–10 AU while embedded in a planetesimal disk having a mass of order $\sim 100\ M_\oplus$ (Fernández & Ip 1984, 1996). Fernández & Ip (1984) argue that Uranus and Neptune would preferentially gain angular momentum (and thus expand their orbits) by scattering planetesimals and lowering their perihelia down to Jupiter and Saturn. Jupiter, being an effective planetesimal ejector, would shrink its orbit as a consequence of the resulting energy and angular momentum losses. However, it should be noted that this argument, while plausible, is not fully supported by their numerical simulations. Those simulations show net orbital expansion by Uranus and Neptune in some instances and orbital decay in others. Individual runs show considerable to-and-fro motion by Neptune. Such evolution would only stir up the planetesimals rather than trapping them at resonances. We note that these simulations were not fully self-consistent, since gravitational interactions were considered only between planets and planetesimals that were on crossing orbits; long-range forces between the planets and the planetesimals were neglected, as were the mutual planet-planet perturbations. Also, the giant planets' gravitational cross sections were artificially increased in order to speed up the system's evolution. This approximate treatment of planet-planetesimal dynamics was necessitated partly because of the limited computer resources available at the time. A more realistic treatment of disk clearing and planet migration is clearly warranted.

The present work revisits the planet migration scenario using more sophisticated numerical techniques to evolve a system of giant planets that is embedded in a disk composed of many low-mass particles. In § 2, we describe the model and test results in detail. Primary results on the giant planets' orbital evolution with disks having different initial masses are given in § 3. Since the planetesimal disk is the source of the Oort cloud, we discuss the implications of our results for the formation of the Oort cloud in § 4. Particles that manage to avoid ejection will reside in what are sometimes called the *classical* and the *scattered* disks, which are characterized in § 5. The role of unmodeled effects such as disk self-gravity and the role of spiral density waves are discussed in § 6, and conclusions are given in § 7.

2. NUMERICAL METHOD

Our model consists of the Sun, the four giant planets Jupiter, Saturn, Uranus, and Neptune, and a population of numerous (N) low-mass particles initially distributed in a disk. Ideally, one would like to have $N \sim 10^{10}$ in order to follow the evolution of this system with a completely self-consistent calculation of the mutual gravitational perturbations and also include the external forcing due to the Galactic tide. However, such a calculation exceeds current computational resources. Instead, as we describe below, we use a fast orbit integrator together with several simplifications to obtain an approximation to the ideal within a reasonable amount of computing time.

In our simulations, all bodies are treated as point masses; thus, the possibility of collisions or accretion is neglected. This approximation is justified during the late stages of giant-planet formation, when the frequency of planet-particle collisions is smaller than the scattering frequency by a factor of the square of the ratio of the planet's physical radius to its Hill radius, which ranges from 10^{-6} for Jupiter to 10^{-8} for Neptune.

The model includes the mutual gravitational forces exerted between the planets, as well as the forces between the planets and the low-mass particles, but the forces among the particles themselves are neglected. This approximation is employed to reduce the computational expense, and it also eliminates the unphysical self-stirring that would otherwise occur in the model disks considered below, which have masses of $M_D = 10$–$200\ M_\oplus$ distributed among just $N = 1000$ particles. Had the particle-particle interactions been included, the relatively small number of N massive disk particles would quickly stir themselves up so much that the resulting system would hardly resemble a planet-forming particle disk. Although this difficulty is avoided by neglecting the particle-particle forces, this approximation also precludes the possibility that the planets might generate spiral density waves in the disk (see § 6).

Dynamical models have shown that particles scattered into wide orbits with semimajor axes $a \gtrsim 3000$ AU become decoupled from the planets as a result of the Galactic tide (Duncan, Quinn, & Tremaine 1987; see also § 4). These distant bodies are deposited in the Oort cloud, which is effected here by simply removing particles from the system when $a > 3000$ AU.

A second-order mixed variable symplectic (MVS) mapping is used to rapidly advance the heliocentric positions and velocities of the planets and low-mass particles as they interact in the Sun's gravitational field. Our implementation follows the algorithm of Wisdom & Holman (1991), with the improvements of Saha & Tremaine (1992). A fixed step size of $\Delta t = 0.4$ yr is used, which is sufficiently short to resolve the orbits of particles that evolve down to perihelia of $q \simeq 3.5$ AU, as well as most encounters between particles and planets. For the latter, the dynamical timescale of a typical scattering event is[1]

$$T^* \simeq \frac{8}{3}\sqrt{\frac{2q^3}{GM_p}}, \tag{1}$$

where M_p is the scattering planet's mass and q is the particle's closest approach distance. Evaluating T^* with q set to each planet's Hill sphere radius shows that $T^* \simeq 4.1$ yr at Jupiter, 10 yr at Saturn, 29 yr at Uranus, and 57 yr at Neptune. Thus the integration time step of $\Delta t = 0.4$ yr is at worst $\frac{1}{10}$ of the dynamical time for orbits that graze Jupiter's Hill sphere. However, an MVS algorithm that

[1] This encounter time is defined as the time to change the particle's true anomaly from $-\pi/2$ to $\pi/2$ for a planet-centered parabolic orbit having a pericenter distance q from the planet.

employs a fixed step size will fail to resolve very close planet-particle encounters that penetrate well within a planet's Hill sphere and will also fail to correctly evolve a very eccentric orbit when the perihelion passage is not well time-sampled (Rauch & Holman 1999). These difficulties are mitigated by the using the following approximations:

1. During a close encounter between a particle and a planet, two-body trajectories are adopted for their relative motion whenever a particle passes sufficiently close to a planet. Experimentation shows that a "sufficiently close" encounter is one that changes the particle's fractional distance from the planet by more than 50%, or varies its planet-centered angular coordinate by more than 90°, during the time step Δt. For particles that are initially in low-eccentricity heliocentric orbits, the two-body approximation is triggered only when a particle approaches within about 10% of the planet's Hill sphere. For more distant encounters, particle trajectories are in fact evolved with greater accuracy using the standard MVS mapping.

2. When a particle evolves into an orbit of sufficiently high eccentricity, its motion during perihelion passage may be poorly time-sampled and the MVS mapping can produce unphysical evolution. For the step size employed here, significant errors accrue in orbits having perihelia $q \lesssim 3.5$ AU.[2] Proper treatment of such orbits is not of minor import, since approximately 30% of the disk particles cycle through the inner solar system with heliocentric distances of $r < 3.5$ AU. A simple, but impractical, solution is to use a step size small enough to resolve all perihelion passages. However, a more practical approach consists of turning off all planetary perturbations while a particle travels interior to a heliocentric distance of $r < 3.5$ AU; this results in a piecewise Keplerian trajectory that is approximately correct. With this approximation, the particle's perturbations upon the planets are still not fully time-sampled, which causes slow drifts in the system's total energy and angular momentum. Numerical experimentation has shown that the most economical and robust solution to this problem requires turning off the particle's perturbations upon the planets while its *perihelion* distance is $q < 3.5$ AU.

The remainder of this section describes a few critical tests of the algorithm in order to demonstrate that the approximations made here do not introduce any artificial orbital evolution of the planets and the particles that is of any significance.

The quality of the orbit integrations may be illustrated with the restricted three-body problem that consists of a massless particle perturbed by a planet on a circular orbit about the Sun. For this system the particle's Jacobi integral $J = E - L_z \Omega_p$ is conserved, where E is the particle's energy, L_z is its component of angular momentum perpendicular to the planet's orbit, and Ω_p is the planet's mean motion. Figure 1 shows the mean fractional variations $\Delta J/J$ that result when integrating 100 particles for 10^4 yr with a Jupiter-mass planet at $a_p = 5$ AU. Squares are shown for

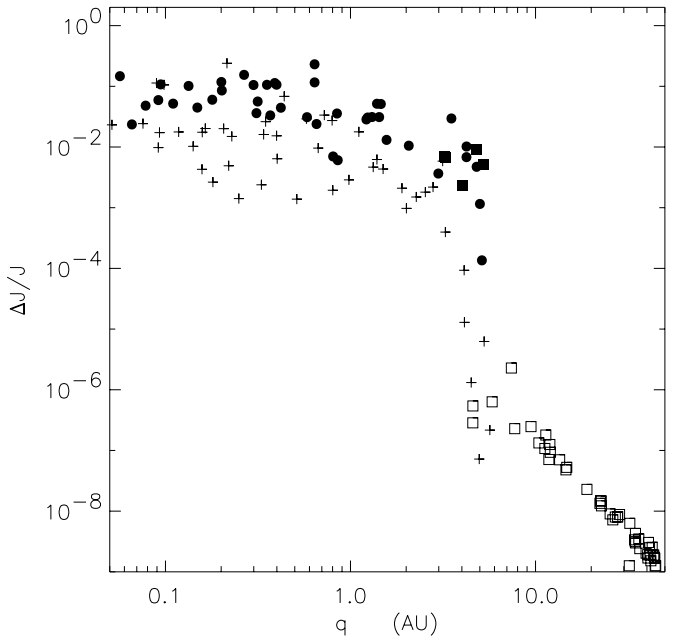

FIG. 1.—Fractional variations in a particle's Jacobi integral J as a function of a particle's perihelion distance q averaged over 10^4 yr. Jupiter lies on a circular orbit at 5 AU, and the integrator step size is $\Delta t = 0.4$ yr. Squares indicate particles having initial eccentricities of $e = 0.1$, inclinations $i = 3°$, and semimajor axes 4 AU $< a <$ 50 AU, while crosses and circles are for eccentric particles having initial perihelia 0.05 AU $< q <$ 6 AU, $a = 6$ AU, and $0° < i < 10°$. Filled circles and squares indicate particles that approached within a Hill radius, or 0.35 AU, of Jupiter.

those particles that start in rather circular orbits near and beyond the planet; these experience a $\Delta J/J \lesssim 10^{-6}$ that decreases with distance provided they have not already made a close approach to Jupiter. Filled squares indicate particles that approach closer than a Hill distance to Jupiter; these experience larger variations in J as a consequence of the close-encounter approximation used here. The remaining particles (*crosses and circles*) are all on Jupiter-crossing orbits, with their perihelia ranging over 0.05 AU $< q <$ 6 AU. Crosses are shown for particles that do not encounter Jupiter, whereas filled circles represent particles that do encounter the planet. The crosses show that $\Delta J/J$ grows inward of Jupiter's orbit as a result of the poor time sampling of the particles' perihelion passages. However, the error $\Delta J/J$ levels off where the integrator turns off the planet's perturbation, and the particle motions are temporarily Keplerian. Failure to implement this procedure would have instead yielded disastrous results inward of about $q \simeq 1$ AU. Shrinking the step size Δt would of course reduce the error in J, but at the expense of precious computer cycles.

An alternate scheme that avoids the growth of numerical errors among low-q particles is to simply remove them when they drop down to a heliocentric distance of $r < 3.5$ AU. Although this procedure inhibits error growth, it is less than desirable since it introduces an unphysical (and very hungry) mass sink into the system. When applying this procedure to the simulations of planet migration described in § 3 (which employ the Keplerian approximation whenever $r < 3.5$ AU), we find that the orbital migration of Saturn, Uranus, and Neptune proceeds radially outward at similar rates. However, the removal of $r < 3.5$ AU particles results

[2] It should be noted that the symplectic integrators of Levison & Duncan (1994) and Duncan, Levison, & Lee (1998) do not suffer this instability when *massless* test particles achieve low-perihelion orbits (H. Levison 1998, personal communication). However, the intervention described above is still required since there is no fully symplectic algorithm that can compute low-perihelion trajectories when the particles carry mass.

in an artificial sunward mass flux that causes Jupiter's orbit to expand rather than shrink. Nonetheless, the fact that the orbital evolution of the outer giant planets is rather insensitive to the treatment of low-q particles adds confidence that the Keplerian approximation employed here is not driving the planet migration reported in § 3. However, enforcing the particles' Keplerian motion inside of $r < 3.5$ AU is still necessary in order to accurately model Jupiter's orbital history.

In the absence of any close encounters between particles and planets, the MVS integrator preserves the system's integrals in the expected manner. However, Figure 1 shows that the close-encounter algorithm used here will not preserve a particle's J to better than one part in 10^3 should it pass within a Hill distance of a planet. This numerical error results in an unphysical diffusion of particle trajectories. This is a concern since the planet migration phenomenon is sensitive to the flux of particles that are scattered and exchanged among the planets (Fernández & Ip 1984; Malhotra 1993).

To judge the effects of numerical diffusion, the restricted three-body problem is again integrated for a system of 100 massless particles that orbit in the vicinity of a Neptune-mass planet in a circular orbit at $a_p = 30$ AU. The particles' initial semimajor axes range over 28.5 AU $< a <$ 31.5 AU and have low initial eccentricities e and inclinations i. For this system, each particle's dimensionless Jacobi integral,

$$J = \frac{a_p}{a} + 2\sqrt{\frac{a}{a_p}\,(1 - e^2)}\,\cos i + O(\mu)\,, \qquad (2)$$

is a conserved quantity. Here a particle's semimajor axis a is in units of a_p and $\mu = 5.15 \times 10^{-5}$ is Neptune's mass in solar units. In this test run, the particles initially have a mean Jacobi integral $\langle J \rangle \simeq 2.998$ with a dispersion $\sigma_J = 5 \times 10^{-4}$. To obtain a physically meaningful measure of the numerical diffusion that occurs in the model, define a threshold value $J_U = 2.989$, which corresponds to an orbit having a perihelion at 20 AU (near Uranus's orbit) and an aphelion at 30 AU (near Neptune's orbit), so that $a/a_p = \frac{5}{6}$ and $e = \frac{1}{5}$. Although this orbit is dynamically forbidden to the test particles, numerical diffusion might allow particles to cross Uranus's orbit, which would result in an unphysical exchange of particles between Neptune and Uranus. The system is integrated for 5×10^7 yr, and at the end of the run, 11 particles have diffused into forbidden Uranus-crossing orbits that have $J < J_U$. The timescale to diffuse into crossing orbits, t_d, is obtained from Figure 2, which shows the particles' average J and their dispersion σ_J versus time. The characteristic diffusion timescale for particles to diffuse across the Jacobi "gap," i.e., the time when $|J - \sigma_J| < J_U$, is $t_d \simeq 2.5 \times 10^7$ yr.

However, it should be noted that a particle's J is not conserved in a multiplanet system. For example, adding a Jupiter at 5 AU to the above simulation will drive these particles into Uranus-crossing orbits having $J < J_U$ at a rate that is about 10 times faster. Since the numerical diffusion rate is considerably slower than the dynamical diffusion that occurs in a multiplanet system, we conclude that the transport of particles between the planets due to numerical diffusion is not significant in these simulations.

As already noted, it is the close encounters between the planets and the planetesimals, and their concomitant exchange of angular momentum, that drive the planet migration process. In our simulations, the planet-particle relative motion during very close encounters is not computed exactly, so any small error in the angular momentum exchange is also reflected in the recoiling planet's orbit. The final test discussed below verifies that the errors in this angular momentum exchange are in fact too small to drive the planet migration described in § 3.

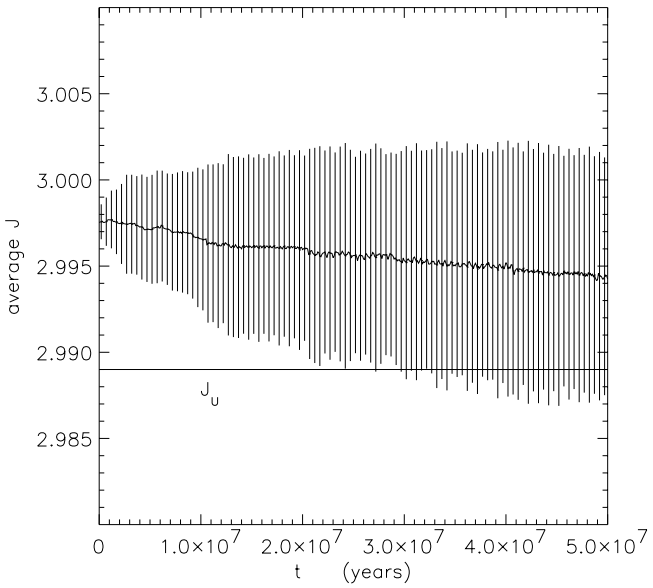

FIG. 2.—A system consisting of Neptune on a circular orbit at $a = 30$ AU and 100 massless particles having initial semimajor axes 28.5 AU $< a <$ 31.5 AU, eccentricities $e = 0.05$, inclinations $i = 0.025$ rad, and Jacobi integrals $2.997 < J < 2.999$, evolved for 5×10^7 yr. The solid curve gives the swarm's average J, with vertical bars indicating the swarm's standard deviation σ_J. The characteristic timescale to diffuse into Uranus-crossing orbits having $J < J_U$ that are dynamically forbidden is $t_d \sim 2.5 \times 10^7$ yr.

The motion of Neptune, as well as several hundred particles of infinitesimal mass m, is integrated at the usual step size of $\Delta t = 0.4$ yr for 200 yr. The same experiment is then repeated using a step size 50 times smaller. Since integration errors decrease with step size, this latter run may be regarded as a much more exact representation of the particle trajectories. Upon differencing the two runs, the error in each particle's velocity relative to the planet, δV, is calculated as the particle exits the planet's Hill sphere. Figure 3*a* shows that most encounters occur at the periphery of the planet's Hill sphere, which result in rather small relative velocity errors. However, the very close encounters having periapse $q \lesssim 0.1 R_H$, which account for 6% of these encounters, result in sizable velocity errors that are of order $\delta V/V \sim 0.1$. The error in the specific angular momentum $\boldsymbol{l}_p$ exchanged between the planet and a scattered particle is $\delta \boldsymbol{l}_p = -m\boldsymbol{r}_p \times \delta \boldsymbol{V}/(M_p + m)$, where $\boldsymbol{r}_p$ is the planet's heliocentric coordinate and M_p is its mass. Figure 3*b* shows a histogram of the z-component of the errors $\delta \boldsymbol{l}_p$, which are distributed about zero. The net specific angular momentum exchanged between the planet and the particle swarm is the sum $L = |\sum \boldsymbol{l}_p|$, and its root mean square error is $\delta L = (\sum \delta \boldsymbol{l}_p^2)^{1/2}$. For the encounters shown in Figure 3, the fractional error in the angular momentum exchanged is only $\delta L/L = 0.016$. The above procedure is also repeated for encounters at Jupiter, which are less well time-resolved, and yields a larger fractional error $\delta L/L = 0.12$. It should be noted that these

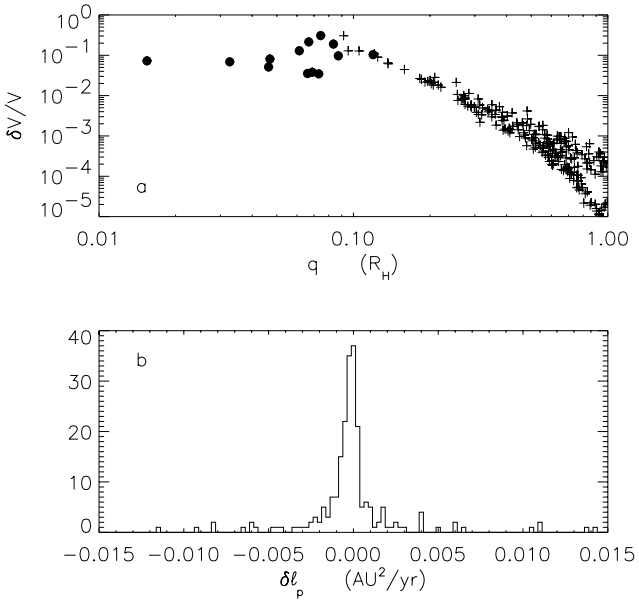

FIG. 3.—(*a*) Fractional error in the relative velocities $\delta V/V$ vs. periapse q (in units of Neptune's Hill radius R_H) of 500 particles after scattering off Neptune. The particles' initial heliocentric orbits were $a \simeq 30$ AU, $e = 0.05$, and $i = 0.025$ rad. Particles that trigger the two-body close-encounter algorithm are indicated by circles. (*b*) Histogram of the z-component of the specific angular momentum errors $\delta \boldsymbol{l}_p$ for each scattering event. The total specific angular momentum exchanged between the planet and the particle swarm is $L = |\sum \boldsymbol{l}_p| = 1.27$ AU^2 yr^{-1}, which has an rms sum $(\sum l_p^2)^{1/2} = 0.64$ AU^2 yr^{-1} and an rms error $\delta L = 0.020$ AU^2 yr^{-1}.

fractional errors decrease for higher relative velocities, which reflects the fact that the two-body approximation, which neglects the Sun's gravity, becomes more accurate with faster encounters. Thus the error in the total angular momentum exchanged between the planet and neighboring particles will steadily decrease as the planet heats up the particle disk. Since these fractional errors are small, we conclude that the close-encounter approximation used here does not drive the planet migration described below.

3. SIMULATIONS OF PLANET MIGRATION

3.1. *Initial Conditions*

In the simulations reported here, we adopted initial planetary orbits similar to those used in previous investigations of planet migration, in which the semimajor axes of Jupiter, Saturn, Uranus, and Neptune are displaced from their present orbits by respective amounts $\Delta a = +0.2$, -0.8, -3.0, and -7.0 AU (Malhotra 1995). The planets are assumed to have their present masses. The initial planetesimal disk is composed of 1000 equal-mass particles distributed in orbits of 10 AU $< a <$ 50 AU such that the disk's inner edge lies just exterior to Saturn and the outer edge lies just beyond the present location of Neptune's 2:1 resonance. The disk surface density σ varies as a^{-1}, $\sigma(a) = 4.0 \times 10^{-3}[M_D/(1\ \mathrm{AU}^2)][(1\ \mathrm{AU})/a]$, where M_D is the total disk mass. Thus, approximately two-thirds of the disk starts exterior to Neptune's initial orbit. Four separate simulations are presented below, in which the disk's initial mass is $M_D = 10$, 50, 100, and 200 $M_\oplus$ and the individual disk particles have masses $m = 0.01$, 0.05, 0.1, and 0.2 $M_\oplus$. An additional 50 massless particles are also distributed between 50 and 100 AU in order to assess the degree of perturbation of a hypothetical part of the Kuiper belt extending well past that which is presently observable.

It should be noted that accretion models advocate an initial disk containing several tens of Earth masses in the 30–50 AU zone in order to form Pluto and QB_1-type Kuiper belt objects (Stern & Colwell 1997; Kenyon & Luu 1998), a scenario that is bracketed by the models explored here.

For those particles that initially lie far from any planets, initial eccentricities of $e_d = 0.01$ and inclinations $i_d = e_d/2$ are adopted. However, particles having a semimajor axis near a planet will already have experienced a history of stirring that results in particle dispersion velocities v_d of the order of the planet's escape velocity at its Hill sphere radius R_H (Ida & Makino 1993), where

$$v_d \sim \sqrt{2GM/R_H}, \quad R_H = [M/(3\ M_\odot)]^{1/3} a\ , \tag{3}$$

with G the gravitational constant, M the planet's mass, and $M_\odot$ the solar mass. Assuming that the particles' inclinations are half their eccentricities, the particles' dispersion velocity is $v_d \simeq [(e_d^2 + i_d^2)GM_\odot/a]^{1/2} \sim e_d(5GM_\odot/4a)^{1/2}$, which corresponds to an eccentricity of $e_d \sim (24/5)^{1/2}(R_H/a)$. With $R_H/a \simeq 0.025$ for both Uranus and Neptune, the particles starting in each planet's heated zone initially have $e_d = 0.06$ and $i_d = 1.^\circ 7$. The adopted half-width of each planet's heated zone is simply each planet's "feeding zone" of $\Delta a = 2\sqrt{3}R_H$ (e.g., Ida & Makino 1993), such that $\Delta a = 1.4$ AU for Uranus and $\Delta a = 2.0$ AU for Neptune when evaluated at their initial heliocentric distances.

For a planet that is embedded in a swarm of identical particles of mass m, dynamical friction will tend to seek an equipartition of energies in the system's epicyclic motions. Again assuming that a planet's inclination obeys $i_p = e_p/2$, its initial eccentricity is then $e_p = e_d(m/M)^{1/2}$, where e_d are the eccentricities of particles in the heated zone. Since Jupiter and Saturn start interior to the particle disk, initially circular and coplanar orbits are adopted for these two planets.

3.2. *Results*

Figure 4 shows the orbital histories of the four giant planets as they scatter the surrounding disk particles in each of the four simulations. We find that the lowest mass disk, $M_D = 10\ M_\oplus$, yields little evolution in the planets' orbits, but the higher mass disks result in significant radial displacements of the planets during the 30 Myr runs. These simulations confirm the expectation that Saturn, Uranus, and Neptune migrate radially outward while Jupiter migrates slightly inward. For a given disk mass, the magnitude of radial migration is largest for Neptune and successively less so for the interior planets. As might be expected, planetesimal disks of greater mass result in planet migration that is larger in magnitude and more rapid, and also more stochastic because of the individual particles' greater mass. Although the planets' orbital eccentricities and inclinations remain small, there is a clear trend toward higher e's and i's at larger disk masses. Since their final e's and i's are largely determined by the numbers and masses of disk particles used in the simulations, their final state have little relation to the giant planets' current e and i configurations. It is worth noting that, in the high-mass disk simulations, the planets pass through a few mutual low-order

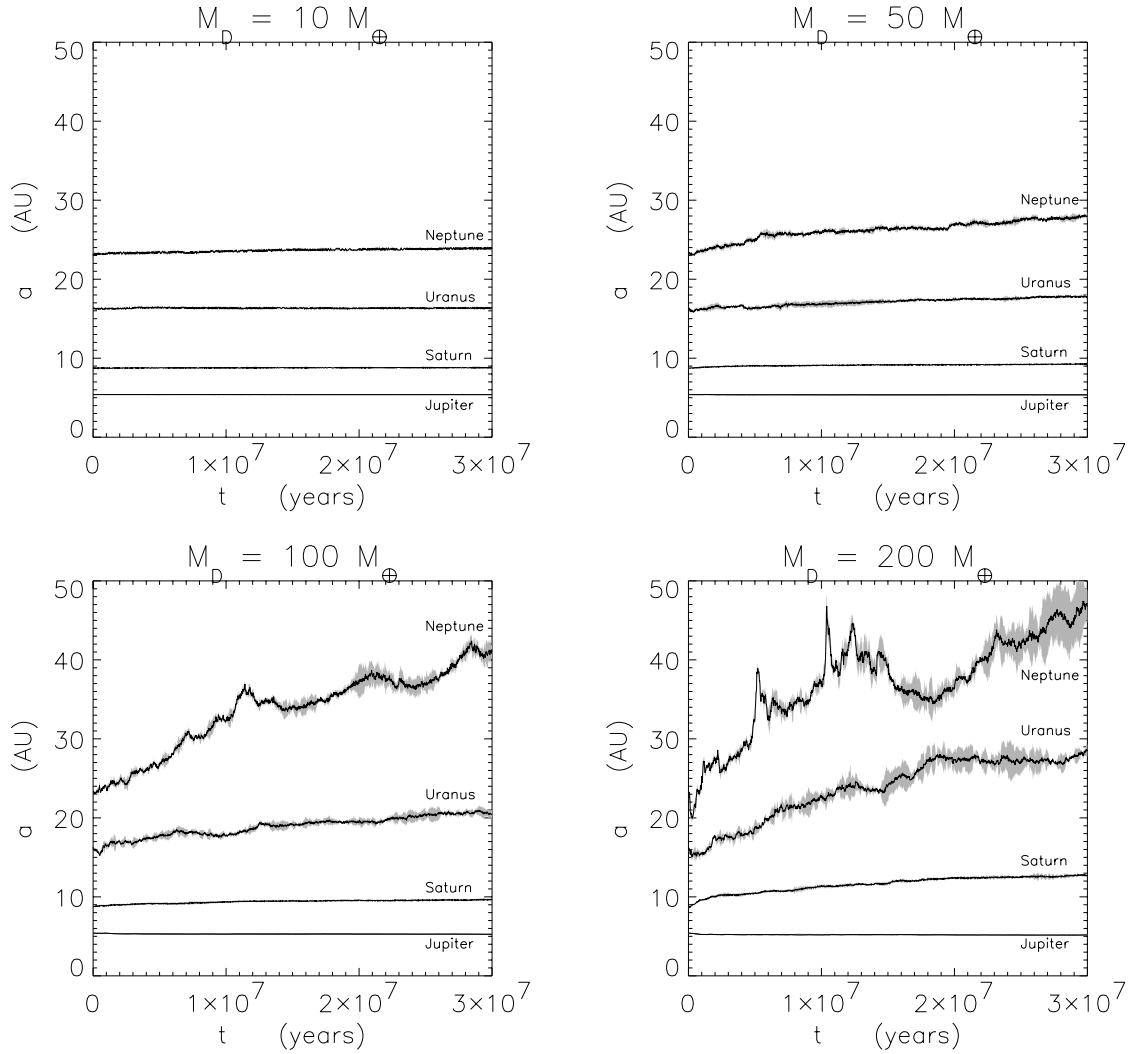

FIG. 4.—Semimajor axes of the giant planets while embedded in planetesimal disks of mass $M_D = 10$, 50, 100, and 200 $M_\oplus$. The boundaries of the gray regions denote the planets' perihelion and aphelion distances.

mean motion resonances, but the planets' orbits do not persist in any resonance-locked configurations. This is not entirely surprising, as the general trend in the orbital evolution is such that the planets are driven toward greater mutual orbital separation, which is not conducive to maintaining a resonance libration (Dermott, Malhotra, & Murray 1988).

Figure 5 shows the state of the $M_D = 50\ M_\oplus$ system at logarithmic time intervals. Large circles indicate the planets' eccentricities and semimajor axes, while small circles and crosses denote particles that have and have not had a close approach to a planet, respectively. Those particles scattered by the planets yet still bound to the Sun tend to have perihelia between the orbits of Saturn and Neptune, as indicated by the two curves. It should be noted that in all of the simulations reported here, the orbital migration of the planets has not ceased by the end of the runs, and that further planet migration will continue (albeit more slowly) past 30 Myr. The simulation of the $M_D = 50\ M_\oplus$ disk is extended to 50 Myr in Figure 6, which shows Neptune slowly expanding its orbit out to 30 AU. These results suggest that in order to actually "park" Neptune at $a = 30$ AU requires an adjustment of parameters toward a slightly lower disk mass, a steeper gradient in the disk's surface density profile, and/or an outer disk edge that lies closer than 50 AU.

3.3. *Discussion*

The disk particles used in all of these simulations are sufficiently massive that their perturbations upon Neptune result in nonadiabatic expansion of that planet's orbit. However, it is evident in Figure 4 that planet migration is smoother when the disk particles have lower mass. Thus, a more realistic simulation employing larger numbers of particles will better resolve the disk-planet perturbations. We expect that such simulations will exhibit orbital migration that proceeds more smoothly. Nearly adiabatic orbital migration is in fact required if Neptune is to efficiently capture particles at its exterior mean motion resonances. Since smooth outward expansion was not realized in these simulations, Neptune did not capture any particles at its mean motion resonances. Thus, the simulated disk's end state cannot be directly compared with the delicate resonant structure that is observed in the Kuiper belt. Neverthe-

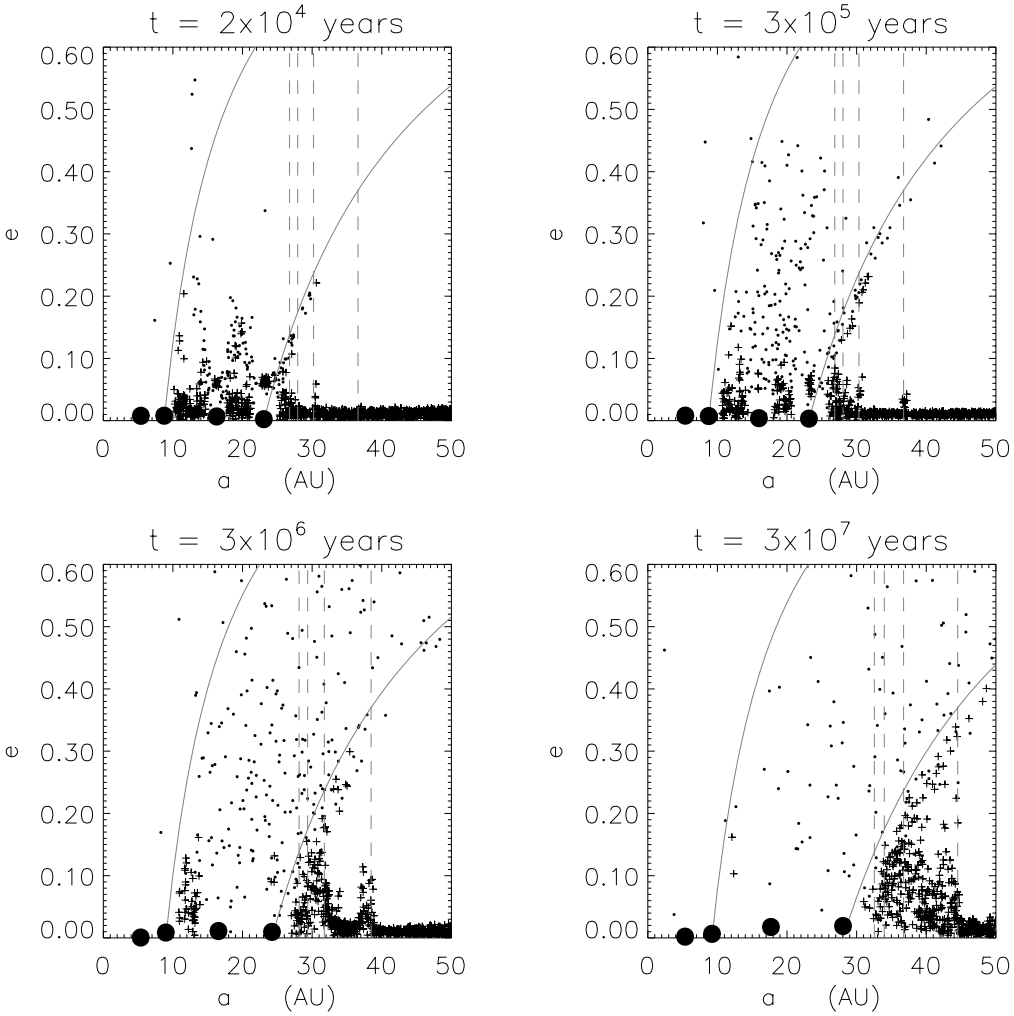

FIG. 5.—Eccentricities e vs. semimajor axes a at logarithmic time intervals for the $M_D = 50\ M_\oplus$ system. Small circles indicate scattered particles that have passed within a Hill radius of a planet, and crosses indicate particles that have not encountered a planet. Large circles denote the planets, and the vertical dashes indicate the location of Neptune's outer four mean motion resonances. Orbits lying above the left curve have perihelia inside of Saturn's orbit, and those above the right curve have perihelia interior to Neptune.

less, these simulations do provide useful constraints on the likely mass of the initial debris disk that may have been present during an early epoch of planet migration.

Figure 7 reports the radial displacement Δa experienced by each planet after $t = 3 \times 10^7$ yr as a function of the initial disk mass M_D. As noted above, Jupiter migrates sunward while the other planets migrate outward in each simulation. The time-averaged torque $T_0 = \Delta L/t$ that drives Neptune by increasing its angular momentum by ΔL during the run time t is shown in Figure 8. This torque, as well as the displacements Δa of Figure 7, should be regarded as an upper limit, since resonance trapping did not occur in these simulations. Had resonance capture been realized here, an opposing torque on the planet would have developed, since the planet must transfer angular momentum to expand the orbits of particles trapped at resonances.

The back-torque due to a ring of mass m that is captured at an exterior $(j + 1):j$ mean motion resonance can be calculated from the rate of change of its angular momentum, $L_m = m[GM_\odot\, a(1 - e^2)]^{1/2}$. Since the resonant torque from the planet expands the ring's semimajor axis at the rate $\dot{a}/a = \dot{a}_p/a_p$ and also pumps up eccentricities at the rate $de^2/dt = (\dot{a}_p/a_p)/(j + 1)$ (Malhotra 1993), the rate of change of L_m is

$$\frac{dL_m}{dt} \simeq \alpha \frac{m}{m_p} T\ , \tag{4}$$

where $\alpha = a_p/a = [j/(j + 1)]^{2/3}$ is the ratio of the semimajor axes of the planet and the resonance site, m_p is the planet's mass, and $T = m_p(GM_\odot\, a_p)^{1/2}\dot{a}_p/2a_p$ is the net torque on the planet, which simplifies to $T = T_0 - dL_m/dt \simeq T_0/(1 + \alpha m/m_p)$. Thus the back-torque from the resonance-captured particles will significantly slow the planet's orbital expansion if the mass trapped at resonance is in excess of the planet's mass, i.e., $m \gtrsim m_p/\alpha$. In a generic system, the strongest exterior mean motion resonance is the 2:1 ($j = 1$, $\alpha = 0.63$), which can be expected to capture the most planetesimal mass. If the capture efficiency is ϵ, then we can estimate that planet migration will slow if

$$\epsilon M_{D,\mathrm{ext}} \gtrsim 1.6 m_p\ , \tag{5}$$

where $M_{D,\mathrm{ext}}$ is the mass of the disk exterior to the planet's initial orbit.

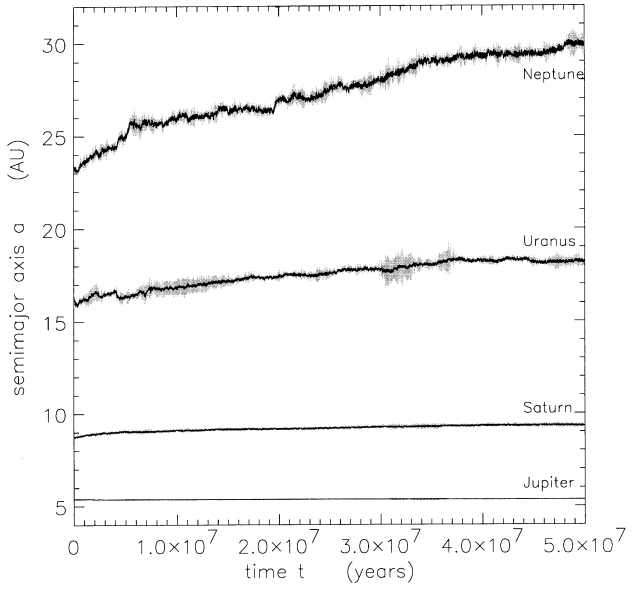

FIG. 6.—Simulation of the $M_D = 50\ M_\oplus$ system extended out to $t = 5 \times 10^7$ yr. Gray indicates perihelion and aphelion distances. Note that Uranus and Neptune pass through a 2:1 mean motion resonance at $t = 3.05 \times 10^7$ yr, which results in a brief eccentricity excitation.

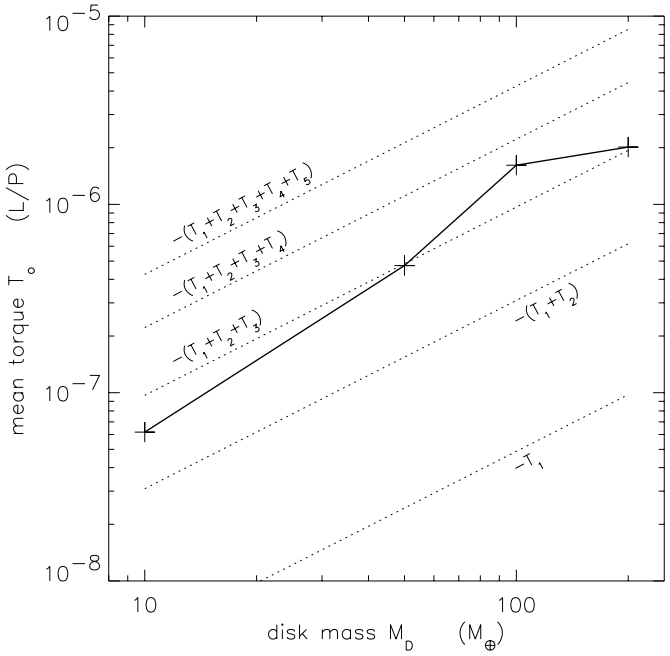

FIG. 8.—Time-averaged torque T_0 on Neptune (*solid curve*), in units of that planet's current angular momentum/orbital period ratio L/P, plotted vs. the disk mass M_D. The dotted curves indicate sums of the resonant disk torque contributions (eq. [6]).

If resonance capture is rather inefficient, then a high-mass disk is simply fuel for planet migration. But if resonance trapping is effective, say, $\epsilon \sim 50\%$, then the planet's migration will slow after the planet has captured a mass m comparable to its own at its exterior resonances. In the disk models considered here (with $M_{D,\mathrm{ext}} \approx \frac{2}{3} M_D$), this would occur only in a high-mass disk with $M_D \gtrsim 80\ M_\oplus$.

If migration by Neptune across a distance $\Delta a \sim 5$–10 AU is to explain the sculpted appearance of the Kuiper belt, then Figures 4 and 7 suggest that the initial planetesimal disk must have had a mass M_D in excess of $10\ M_\oplus$ (since a lower mass disk results in insufficient planet migration that proceeds too slowly) but likely less than $\sim 100\ M_\oplus$ (since such a high-mass disk would likely produce additional giant planets). A more precise disk mass estimate requires detailed knowledge of the disk's radial extent and the particulars of the disk surface density variations $\sigma(a)$.

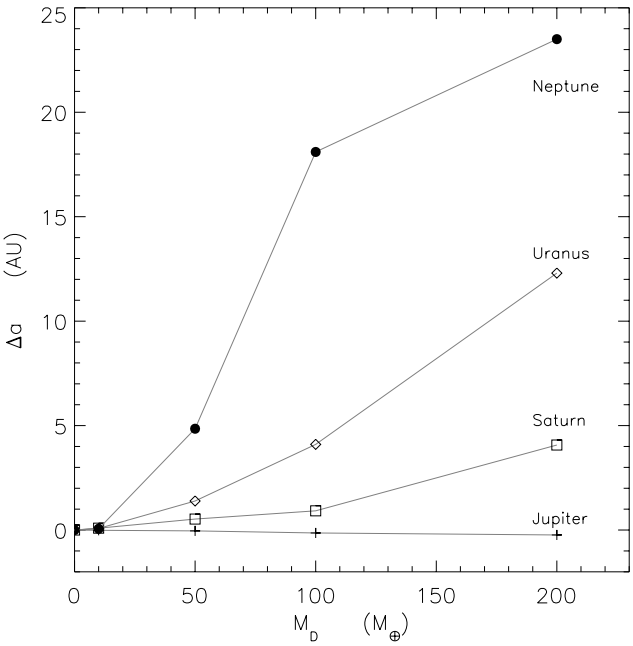

FIG. 7.—Radial displacement Δa vs. disk mass M_D for each planet after $t = 3 \times 10^7$ yr.

4. THE OORT CLOUD MASS

The observed flux of long-period comets provides a constraint on the present mass of the Oort cloud. In this section, we use the results of our numerical simulations to estimate the mass of its progenitor, the primordial planetesimal disk in the outer solar system.

After adjustment for the efficiency of comet detections, it is estimated that ~ 63 long-period comets per year pass through the inner solar system with perihelia $q < 4$ AU (Everhart 1967). This flux stems entirely from the Oort cloud; objects originating in the Kuiper belt evolve instead into the short-period Jupiter-family comets (Levison 1996). Dynamical models of the Oort cloud, when adjusted to match the flux of long-period comets, require a reservoir of $N_{\mathrm{OC}} \sim 1.6 \times 10^{13}$ bodies (Heisler 1990).[3] Multiplying by the typical comet mass yields the total mass of the Oort cloud. Based upon an admittedly uncertain relationship between cometary brightness and size, Weissman (1996) concludes that the mean comet mass is of order $\sim 10^{16}$ g, indicating an Oort cloud mass of order $M_{\mathrm{OC}} \sim 27\ M_\oplus$. However, this mass estimate should be regarded as uncertain by at least an order of magnitude, since it relies upon a host of uncertain quantities such as the efficiency of comet detections and the comet brightness-mass relationship, as

[3] The Heisler (1990) Oort cloud model shows that a reservoir of 10^{11} comets will produce a flux of 0.2 comets per year having $q < 2$ AU. To match the observed flux of comets with $q < 4$ AU, multiply this population by $63/(2 \times 0.2)$.

well as uncertainties in the Oort cloud perturbations (e.g., the strength of the Galactic tidal field and the frequency of stellar encounters).

The dynamics of the Oort cloud is succinctly summarized by Duncan et al. (1987). Unless a particle is otherwise ejected from the system, planetary perturbations cause its semimajor axis to diffuse both inward and outward while keeping its perihelion locked in the giant-planet region of the solar system. However, a more distant particle is susceptible to perturbations by the Galactic tide and passing stars, which cause its perihelion to diffuse on a timescale that varies as $t_q \propto a^{-2}$. Those particles reaching 3×10^3 AU $\lesssim a \lesssim 2 \times 10^4$ AU that have had their perihelia raised well beyond the orbit of Neptune are thus decoupled from the planets and are usually identified as *inner* Oort cloud comets. However, the perihelia of more distant bodies diffuse more rapidly, and those with 2×10^4 AU $\lesssim a \lesssim 10^5$ AU that reside in the *outer* Oort cloud are in fact more likely to diffuse back into the inner solar system and become observable as new long-period comets. It is this flux of new comets that provides an important constraint on the amount of mass driven from the initial disk that has managed to avoid ejection during the last 4.5 Gyr.

Estimates of the Oort cloud mass may be inferred from the data given in Table 1. The quantity f_{3k} is the fraction of the *dynamically active* disk that diffuses into the Oort cloud at $a > 3 \times 10^3$ AU during each simulation. The dynamically active disk is that part of the disk where particles are likely to be perturbed into Neptune-crossing orbits over the age of the solar system. Long-term integrations of Kuiper belt orbits show that particles in the active disk have semimajor axes $a \lesssim 1.4a_N$, where a_N is Neptune's semimajor axis (Duncan, Levison, & Budd 1995). The mass of the dynamically active disk, M_{ad} (Table 1), is defined here as the total mass of ejected particles plus all survivors having $a \lesssim 1.4a_N$, which are presumably in unstable orbits. Also given is f_h, which is the fraction of the active disk that has been ejected from the system. Figure 9 displays f_{3k} and f_h versus time for the $M_D = 100\ M_\oplus$ run. What is most striking is that at the end of all four runs both f_{3k} and f_h vary little among the different simulations (Table 1). This indicates that the total mass deposited in the Oort cloud depends only on the mass of the disk that lies within the planets' gravitational reach and is not very sensitive to the orbital histories of the migrating planets.

Ultimately, all particles starting in the dynamically active disk are either ejected, deposited in the Oort cloud, or in some instances accreted by the planets. Although the latter outcome is not modeled here, impacts may be assessed ex post facto using the collision probabilities of Öpik (1951). After summing the probability of each particle striking each planet, we find that ~15 of the 1000 particles would have struck the giant planets during each simulation, with roughly half these impactors striking Jupiter. Such impacts would have contributed no more than ~2% to any planet's mass, so the neglect of particle-planet collisions is justified. It is also worth noting that a few percent of the disk passes through the terrestrial zone, as is indicated by the $f_{q<3.5}$ curve of Figure 9, which shows the instantaneous disk fraction having perihelia inside of 3.5 AU. In these simulations typically ~30% of all disk particles have brief episodes with $q < 3.5$ AU. These findings are consistent with earlier studies showing that planetesimals scattered during the epoch of disk clearing and planet migration may have contributed significant numbers of impactors during the late, heavy bombardment of the terrestrial planets (Wetherill 1975; Shoemaker & Wolfe 1984).

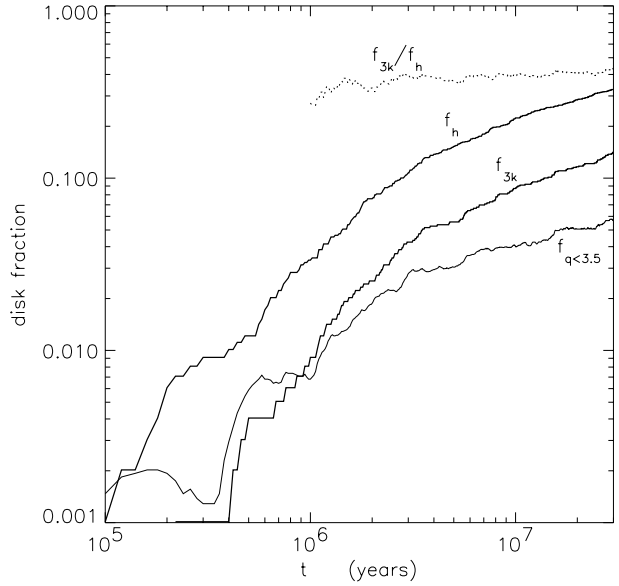

FIG. 9.—Fraction of the active disk that is ejected into hyperbolic orbits, f_h, vs. time t for the $M_D = 100\ M_\oplus$ simulation. The disk fraction that is scattered into the Oort cloud with $a > 3000$ AU is f_{3k}, and $f_{q<3.5}$ is the instantaneous disk fraction having perihelia $q < 3.5$ AU. Note the near-constancy of the ratio $f_{3k}/f_h \simeq 0.4$. Curves for the other runs are quite similar.

TABLE 1

OORT CLOUD MASSES

M_D ($M_\oplus$)	f_{3k}	f_h	f'_{3k}	f'_h	M_{ad} ($M_\oplus$)	M_{OC} ($M_\oplus$)
10	0.097	0.355	0.215	0.785	5.7	0.41
50	0.143	0.364	0.282	0.718	35	3.3
100.....	0.142	0.327	0.303	0.697	99	10
200.....	0.141	0.369	0.276	0.724	200	18

Table 1 shows that in the four simulations the active disks are depleted by a factor $f \equiv f_{3k} + f_h \simeq 50\%$ after $t = 3 \times 10^7$ yr. It should be noted that the family of $f(t)$ curves is described well by a power law $f \propto t^{0.44}$. This indicates that a fully evolved system having $f \to 1$ requires an integration lasting the duration of the disk's dynamical lifetime, $\tau_d \sim 1.5 \times 10^8$ yr, which is beyond our computational means. However, it is straightforward to extrapolate the formation of the Oort cloud from the simulations at hand. Figure 9 shows that the ratio $f_{3k}/f_h \sim 0.4$ remains relatively constant during the bulk of the run. This relation permits an extrapolation to a fully evolved state of the system having $f'_{3k} + f'_h \to 1$, where the primes denote final extrapolated values. Assuming $f'_{3k}/f'_h = f_{3k}/f_h$ over the age of the solar system, the extrapolated fractions become $f'_h = (1 + f_{3k}/f_h)^{-1} \simeq 0.73$ and $f'_{3k} = 1 - f'_h \simeq 0.27$; these values are also given in Table 1. Since these disk fractions are both number as well as mass fractions, the extrapolated planetesimal mass that is initially deposited in the inner Oort cloud is $f'_{3k} M_{ad}$. However, the Galactic tide will subsequently strip away comets that diffuse past $a \gtrsim 10^5$ AU, and passing stars will eject others. Numerical studies show that

these external perturbations acting over the age of the solar system will reduce the Oort cloud mass to about a third of its initial value (Duncan et al. 1987). Thus the final Oort cloud mass reported in Table 1 is $M_{OC} = f'_{3k} M_{da}/3$, and it is also displayed as the solid curve in Figure 10 as a function of the initial disk mass M_D.

The nebula origin of the Oort cloud is given by the solid curve in Figure 11, which shows a histogram of the Oort cloud particles' initial semimajor axes for the $M_D = 50\ M_\oplus$ disk; after $t = 3 \times 10^7$ yr, the planetary configuration in this system most resembles the solar system. Since the inner edge of our model disks is truncated at 10 AU, any Oort cloud mass originating in interior orbits is still unaccounted for. We estimate this contribution after the fact by evolving a system of four giant planets in their present configuration plus an annulus of 153 massless test particles having an initial $\sigma \propto a^{-1}$ surface number density a between 4 and 10 AU. Their Oort cloud contribution is given by the dashed curves in Figures 10 and 11. Evidently, all parts of the giant-planet domain contribute mass to the Oort cloud. These findings are in agreement with those of Weissman & Levison (1997), who reported that a small fraction of Oort cloud bodies can originate from orbits interior to Jupiter and thus have asteroidal rather than cometary compositions.

If the initial disk had a mass $10\ M_\oplus \lesssim M_D \lesssim 100\ M_\oplus$ (§ 3), then Figure 10 indicates that the resulting Oort cloud mass is $0.5\ M_\oplus \lesssim M_{OC} \lesssim 11\ M_\oplus$. This mass estimate must be qualified for two reasons. For the lower mass disks, $M_D \leq 50\ M_\oplus$, the mass estimate M_{OC} as given in Figure 10 is likely an underestimate because in deriving it we have not accounted for the possibility that Neptune can migrate deeper into the disk as the system evolves further on time-scales longer than ~ 50 Myr, thus allowing additional material to be injected into the Oort cloud. (This does not affect the higher disk mass simulations, since Neptune's gravitational reach has already swept across the entire disk in the higher mass runs.) For the higher mass disks, M_{OC} is likely overestimated in Figure 10 because resonance trapping tends to slow planet migration and may reduce the mass encountering the planets and, thus, the mass deposited in the Oort cloud. We note that an Oort cloud having a total mass $M_{OC} \sim 5\ M_\oplus$ and a population $N_{OC} \sim 1.6 \times 10^{13}$ comets (Heisler 1990) suggests that a characteristic Oort cloud comet has a radius of ~ 1 km for a density of ~ 0.5 g cm^{-3}.

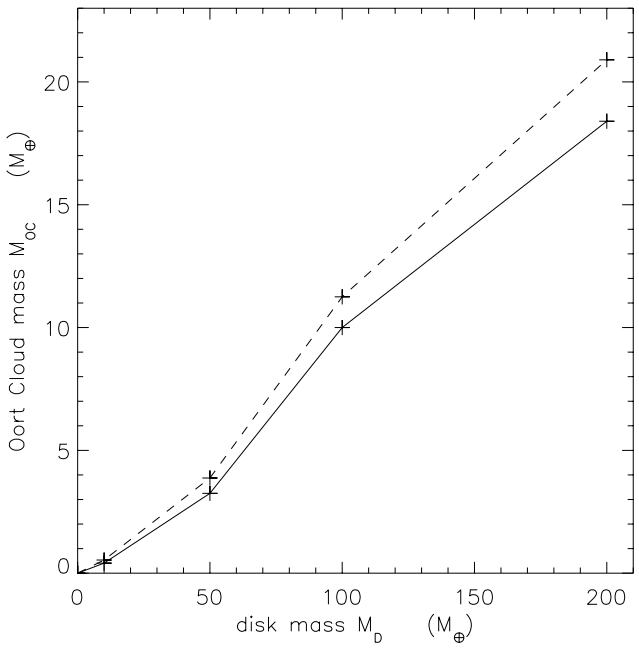

FIG. 10.—Extrapolated mass of the Oort cloud mass M_{OC} as a function of the initial disk mass M_D. The dashed curve includes contributions by massless test particles originating in the 4 AU $< a <$ 10 AU part of the disk that is modeled separately. However, each one of these particles, when deposited in the Oort cloud, is assumed to contribute the same individual mass as its compatriot particles that are employed in the simulations of Fig. 4.

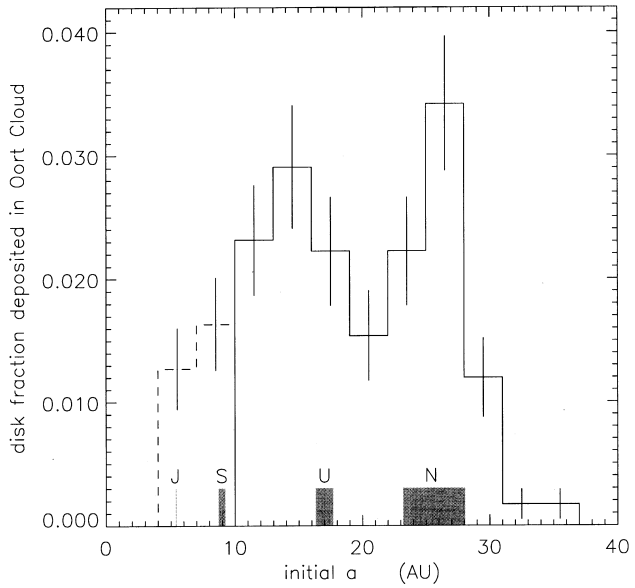

FIG. 11.—Local disk fraction deposited in the Oort cloud vs. initial semimajor axis a for the $M_D = 50\ M_\oplus$ simulation. The data are obtained at time $t = 3 \times 10^7$ yr and then extrapolated to a fully evolved state by multiplying by $f'_{3k}/f_{3k} = 1.97$. The gray bars show the extent of radial migration by each planet. The 4 AU $< a <$ 10 AU component (*dashed curve*) is obtained from a separate integration, and $\sqrt{N}$ errors are assumed.

5. THE RESONANT, STIRRED, AND SCATTERED KUIPER BELT COMPONENTS

Although the giant planets scatter planetesimals throughout the entire solar system, a large gap in orbital phase space will develop, as illustrated by Figure 12. This gap is easily explained via the restricted three-body problem, which shows that a planet on a circular orbit will scatter a massless body in a manner that preserves the particle's Jacobi integral J (eq. [2]). Particles originating in a cold disk in the vicinity of the planet have semimajor axes $a \simeq a_p$ and $J \simeq 3$. Once scattered, these particles will have eccentricities defined by the curve $e_{J=3}$ (Fig. 12), assuming $i = 0$. It has also been shown that a planet of low eccentricity will repeatedly scatter particles along a curve that approximately preserves $J \simeq 3$ (Ida & Makino 1993). Thus, when several planets are present, those interior to Neptune can loft particles into high-eccentricity Neptune-crossing orbits and ultimately fill the $e > e_{J=3}$ region of phase space. Those particles in the high-eccentricity $e \gtrsim e_{J=3}$ orbits of Figure 12 are referred to as the *scattered disk* (e.g., Duncan & Levison 1997). The region occupied by bodies of lower eccentricity beyond ~ 35 AU is sometimes referred to in recent literature as the "classical" Kuiper belt; the eccen-

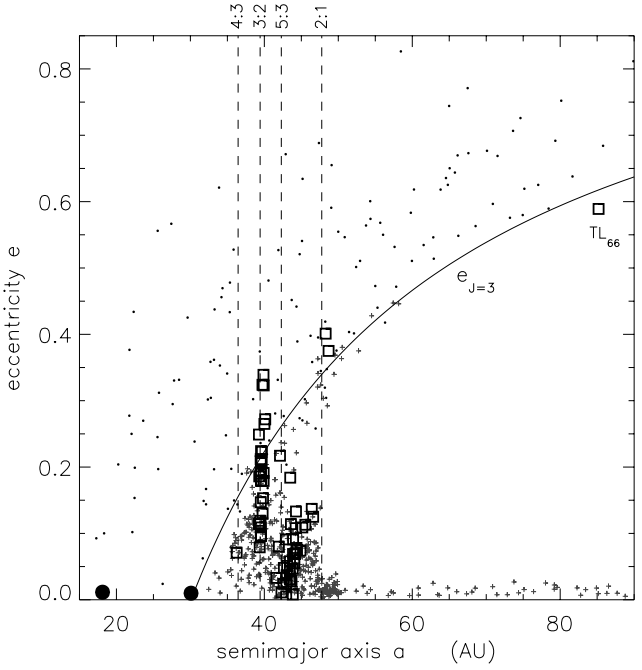

FIG. 12.—Eccentricity e vs. semimajor axis a at time $t = 5 \times 10^7$ yr for the $M_D = 50\ M_\oplus$ simulation. Large circles indicate Uranus and Neptune, small circles indicate scattered particles that have passed within a Hill distance of a planet, and crosses denote particles that have not had a close planetary encounter. The dashed lines indicate Neptune's four outermost mean motion resonances, and the $e_{J=3}$ curve satisfies eq. (2) with $i = 0$. Boxes denote observed KBOs having well-determined orbits (from Marsden 1999), and the scattered object 1996 TL_{66} is indicated.

tric, resonant objects (including the so-called Plutinos at Neptune's 3:2 resonance) may be considered a distinct dynamical subclass of the latter population.

Although Figure 12 shows the scattered and classical disks after only 5×10^7 yr, Duncan & Levison (1997) have integrated test particle orbits for the age of the solar system. They find that while most particles in the scattered disk are removed in less than the age of the solar system, about 1% of the scattered particles survive for longer times (perhaps by acquiring protection via the Kozai mechanism [Kozai 1962] or by sticking near mean motion resonances). In the absence of disk stirring by any other large, distant perturbers, we note that the phase-space gap between the classical and scattered disk will persist over the age of the solar system. This gap should become evident as deeper observations begin to peer beyond Neptune's 2:1 resonance.

Until very recently, no KBOs were known to orbit at Neptune's 2:1 resonance, in apparent conflict with the prediction of the planet migration/resonance-sweeping theory that KBO populations at the 2:1 and 3:2 should be similarly abundant and have comparable eccentricities (Malhotra 1995). As this paper was being written, we learned that two KBOs, 1997 SZ_{10} and 1996 TR_{66}, have been identified as librating in the 2:1 Neptune resonance (Marsden 1999).[4] We note that these two KBOs were formerly identified in Neptune's 5:3 and 3:2 resonances, and that their orbits were revised to the 2:1 resonance only after observations spanning two and three oppositions, respectively. Clearly, orbit-fitting biases and observational incompleteness remain in the current census of the Kuiper belt. A robust test of the planet migration/resonance-sweeping theory requires a larger observational sample of reliable KBO orbits.

Morbidelli & Valsecchi (1997) offer an alternative explanation for the structure in the Kuiper belt. They suggest that if a stationary Neptune had scattered a couple of Earth-mass planetesimals (i.e., LNSPs, or "large Neptune-scattered planetesimals") outward, these massive bodies could have stirred up KBO eccentricities to $e \sim 0.2$, similar to those observed for KBOs at Neptune's 3:2 resonance. Gravitational scattering can indeed insert KBOs into, as well as remove objects from, mean motion resonances, but scattered objects tend to librate at resonance with such large amplitudes that close encounters with Neptune become possible and long-term orbital stability is precluded (Levison & Stern 1995). Therefore, an additional sequence of collisions and/or scattering events is required in order for particles to diffuse to stable, small-amplitude librating orbits. Only the fortunate few would survive this process, so the yield of KBOs scattered into stable $e \sim 0.2$ orbits at the 3:2 resonance would be much smaller than that which might otherwise be acquired by means of adiabatic orbit expansion and resonance sweeping by Neptune. Morbidelli & Valsecchi (1997) also point to the $e \sim 0.1$ KBOs that reside between the 3:2 and 2:1 resonances as additional evidence for LNSPs. But resonance capture is not entirely efficient, and similar eccentricities are also achieved as Neptune's orbit expands and its 2:1 resonance sweeps across the disk and stirs up eccentricities (Fig. 12).

A census of KBOs beyond Neptune's 2:1 resonance (at 48 AU) would permit an evaluation of possible stirring by hypothetical LNSPs. If the natal planetesimal disk does extend past 48 AU, then Figure 12 shows that planet migration will produce a stirred zone interior to the 2:1 yet leave the disk exterior to the 2:1 relatively undisturbed. However, an abundant population of eccentric KBOs beyond the 2:1 would suggest a history of additional stirring by other unseen perturbers (though this would not preclude an episode of planet migration).

6. DISK SELF-GRAVITY AND THE ROLE OF SPIRAL DENSITY WAVES

As noted earlier, our simulations neglect the planetesimal disk's self-gravity in order to inhibit an unphysical degree of self-stirring. The consequences of disk self-gravity could be better studied only by simulating disks composed of many more lower mass particles. In this section, we discuss the possible consequences of the disk's self-gravity.

If the local disk mass exceeds the mass of a nearby planet (as is the case for Neptune in most of the simulations considered here), it is the disk's gravity that can control the rates at which the perihelia and nodes of both the planet and the disk particles precess and/or regress (Ward 1981). Secular resonances are sites in the disk where a planet's perihelion/node varies at the same rate as the disk particles', and high eccentricities and inclinations can be excited at these resonances. As planets sculpt the disk and cause its surface density to evolve over time, the location and strength of secular resonances will shift. Although radial drifts in the location of secular resonances might alter the details of how a planet depletes the disk as it excites particles into crossing orbits, this issue is likely of lesser importance when compared with the mean motion resonances.

[4] See http://cfa-www.harvard.edu/iau/lists/TNOs.html.

In particular, a planet that is embedded in a self-gravitating disk can launch spiral density waves at its mean motion resonances. Numerous examples of this phenomenon exist in Saturn's rings, which exhibit density waves driven by orbiting satellites. The gaps in these rings reveal a history of angular momentum exchange between ring material and satellites, and similar exchanges are expected of planet-forming systems. When Neptune launches density waves at an exterior $(j+1):j$ mean motion resonance, the disk exerts the torque T_j on the planet, which opposes its radial migration:

$$T_j = \frac{j\pi^2\sigma\psi^2}{r\,dD/dr} \simeq -\frac{64\pi j^3}{75(j+1)}\,\mu_p^2\,\mu_d\,M_\odot(a_p\Omega_p)^2 \qquad (6)$$

(Goldreich & Tremaine 1980). Here $\psi \simeq -8j\mu_p(r\Omega)^2/5$ is the planet's forcing function, μ_p is the planet's mass in solar units, Ω is the disk's mean motion, D is the frequency difference from exact resonance, which has the gradient $r\,dD/dr \simeq -3(j+1)\Omega^2$, and the preceding quantities are evaluated at resonance $r = (1+j^{-1})^{2/3}a_p$ with a_p and Ω_p the planet's semimajor axis and mean motion (Hahn, Ward, & Rettig 1995). The dimensionless "disk mass" is $\mu_d \equiv \pi\sigma(a_p)a_p^2/(1\ M_\odot) \simeq 1.1\times10^{-6}[M_D/(1\ M_\oplus)]$ for the disk simulations that have $\sigma(a_p) = 1.3\times10^{-4}M_D/(1\ \mathrm{AU}^2)$. Figure 8 sums the torques T_j due to Neptune's outer $j = 1$–5 resonances for comparison with the nonresonant torque T_0 that drives Neptune's orbit expansion.

Evidently, the resonant disk torques can inhibit Neptune's outward migration if the disk admits a wave response at the $j \gtrsim 3$ resonances. It should be noted that these torques are also operative in non–self-gravitating disks (Lissauer & Espresate 1998), and similar torques also slow orbit expansion when resonance trapping is effective (§ 3.3). But when trapping is not of concern, the resonant torques in a nongravitating disk shut off once particle eccentricities become excited (Lissauer & Espresate 1998). However, in a self-gravitating particle disk, density waves transport the planet's forced disturbance downstream of the resonance in the direction of the planet's orbit. As long as wave action is sustained, particles at resonance maintain low eccentricities and the resonant disk torque can oppose planet migration.

There are two ways in which the propagation of density waves might be inhibited in particle disks. In a disk that is populated by comet-sized (or larger) planetesimals, dissipative forces such as gas drag or viscosity due to interparticle collisions are insufficient to damp out density waves (e.g., Hahn et al. 1995). In this case, density waves reflect at a Q-barrier in the disk and return to the launch zone, where they are reabsorbed by the particles at resonance (Toomre 1969). This absorption of the returning waves' energy will steadily heat the disk and can eventually shut off subsequent wave generation. A second way to defeat waves is via stirring by larger bodies, which also heats the disk and inhibits wave propagation. Consequently, the resonant torque that the particle disk exerts on Neptune will delay the onset of orbit expansion until the disk becomes too stirred to sustain density waves at its $j \gtrsim 3$ resonances.

7. CONCLUSIONS

The existence of the Oort comet cloud, as well as the Kuiper belt, suggests that there was once a residual planetesimal disk of mass $\sim$10–100 $M_\oplus$ in the vicinity of the giant planets following their formation. Further, any inefficiencies in the formation of the giant planets' cores implies additional disk mass. The eventual clearing of this planetesimal population involves a substantial exchange of orbital energy and angular momentum with the planets, implying that the present locations of the giant planets are not necessarily their formative ones. We have numerically simulated the evolution of a system of four giant planets embedded in a planetesimal disk of mass ranging from 10 to 200 $M_\oplus$. Our numerical simulations show a gradual increase in the mutual separation of the planets' orbits as the disk is dispersed via gravitational scattering by the planets. Higher disk masses yield planetary orbital migration that is faster and larger in magnitude. If planet migration and resonance trapping are invoked to explain the eccentricities of Pluto and its cohort of Kuiper belt objects at Neptune's 3:2 mean motion resonance, then these simulations show that a disk mass of order $M_D \sim 50\ M_\oplus$ is required to expand Neptune's orbit the requisite distance of $\Delta a \sim 7$ AU to pump up Plutino eccentricities to $e \sim 0.3$. Such an episode of planet migration implies that the solar system was more compact in the past, with the initial Jupiter-Neptune separation having been smaller by about 30%. This finding also confirms the disk mass estimate previously obtained by Malhotra (1999).

Our model disk-planet systems behave similarly to other disk systems that experience a gravitational or viscous torque (e.g., Lynden-Bell & Kalnajs 1972; Lynden-Bell & Pringle 1974), which causes angular momentum to be carried radially outward (in this application, by the outer three planets) while disk particles deliver mass radially inward. However, these particles tend to be ejected upon reaching Jupiter's orbit, which accounts for that planet's slight orbital decay.

Since our simulations neglected the disk's self-gravity, collective effects such as density waves are precluded. A planet embedded in a self-gravitating planetesimal disk will tend to launch spiral density waves at its resonances. The torque due to wave generation is sufficient to oppose Neptune's orbital expansion as long as the disk remains dynamically cold enough to admit a wave response from its $j \simeq 3$ or higher resonances. Such an episode of wave generation will delay the onset of planet migration until the disk's wave response is defeated.

The bulk of the disk particles deposited in the Oort cloud originate in the vicinity of the Saturn-Neptune region of the solar nebula. Assuming that Galactic tides and passing stars decouple particles from the planetary system when they achieve a semimajor axis of $a > 3000$ AU, and that these perturbations also remove about two-thirds of the Oort cloud over the age of the solar system (Duncan et al. 1987), we estimate that about $M_{\mathrm{OC}} \sim 12\ M_\oplus$ of the $M_D = 50\ M_\oplus$ disk is initially emplaced in the Oort cloud, of which $\sim$4 $M_\oplus$ will persist to the present age of the solar system.

Because of the fact that the disks simulated here were sparsely populated by particles having masses $m = 0.01$–0.2 $M_\oplus$, their vigorous scattering caused the planets' orbits to evolve nonadiabatically such that resonance trapping of KBOs was inhibited. However, previous studies have shown that adiabatic orbit expansion by Neptune can account for the abundance of eccentric KBOs that are known to orbit at Neptune's 4:3, 3:2, 5:3, and 2:1 mean motion resonances (Malhotra 1995). Unless there are (or were) additional unseen, distant perturbers, any primordial

KBOs beyond Neptune's 2:1 resonance should reside in nearly circular, low-inclination orbits.

The planet migration/resonance-trapping phenomenon might also have applications in extrasolar planetary systems. The most visible component of an extrasolar planetary system is likely its dust, which should be most abundant when planets and planetesimals are colliding, accreting, and eroding. Dusty circumstellar disks and rings are known to orbit the stars β Pictoris, Formalhaut, HR 4796A, 55 Cancri, and ϵ Eridani (Smith & Terrile 1984; Greaves et al. 1998; Trilling & Brown 1998; Koerner et al. 1998; Holland et al. 1998; Smith et al. 1998). In some of these systems, collisions and/or radiation forces will remove the observed dust on a timescale shorter than the age of the parent star. The presence of dust thus suggests an additional source—perhaps dust generation due to collisions by unseen planetesimals that reside in the disk. Any planets that might form within this environment will deplete the disk region that lies within their gravitational reach, which could account for these disks' central gaps. However, an episode of planetesimal disk clearing would also drive planet migration, which can concentrate planetesimals at the outermost planet's exterior mean motion resonances. Since the collision frequency and, hence, the dust generation rate varies as the square of the planetesimal density, one might speculate that this mechanism is also responsible for the formation of dust rings observed around ϵ Eri, Formalhaut, and HR 4796A.

The authors thank Derek Richardson for a careful review of this paper. This paper is contribution 966 from the Lunar and Planetary Institute, which is operated by the Universities Space Research Association under NASA contract NASW-4574. This research was supported in part by NASA's Origins of Solar Systems research program.

REFERENCES

Dermott, S. F., Malhotra, R., & Murray, C. D. 1988, Icarus, 76, 295
Duncan, M. J., & Levison, H. F. 1997, Science, 276, 1670
Duncan, M. J., Levison, H. F., & Budd, S. M. 1995, AJ, 110, 3073
Duncan, M. J., Levison, H. F., & Lee, M. H. 1998, AJ, 116, 2067
Duncan, M., Quinn, T., & Tremaine, S. 1987, AJ, 94, 1330
Everhart, E. 1967, AJ, 72, 1002
Fernández, J. A. & Ip, W.-H. 1984, Icarus, 58, 109
———. 1996, Planet. Space Sci., 44, 431
Goldreich, P., & Tremaine, S. 1980, ApJ, 241, 425
Greaves, J. S., et al. 1998, ApJ, 506, L133
Hahn, J. M., Ward, W. R., & Rettig, T. W. 1995, Icarus, 117, 25
Heisler, J. 1990, Icarus, 88, 104
Holland, W. S., et al. 1998, Nature, 392, 788
Ida, S., & Makino, J. 1993, Icarus, 106, 210
Jewitt, D., Luu, J., & Trujillo, C. 1998, AJ, 115, 2125
Kenyon, S. J., & Luu, J. X. 1998, AJ, 115, 2136
Koerner, D. W., Ressler, M. E., Werner, M. W., & Backman, D. E. 1998, ApJ, 503, L83
Kozai, Y. 1962, AJ, 67, 591
Levison, H. F. 1996, in ASP Conf. Ser. 107, Completing the Inventory of the Solar System, ed. T. W. Rettig & J. M. Hahn (San Francisco: ASP), 173
Levison, H. F., & Duncan, M. J. 1994, Icarus, 108, 18
Levison, H. F., & Stern, S. A. 1995, Icarus, 116, 315
Lissauer, J. J., & Espresate, J. 1998, Icarus, 134, 155
Lynden-Bell, D., & Kalnajs, A. J. 1972, MNRAS, 157, 1
Lynden-Bell, D., & Pringle, J. E. 1974, MNRAS, 168, 603
Malhotra, R. 1993, Nature, 365, 819
———. 1995, AJ, 110, 420
———. 1998, in Lunar and Planetary Science XXIX (Houston: Lunar Planet. Inst.), No. 1476
———. 1999, Planet. Space Sci., in press
Marsden, B. 1999, List of Transneptunian Objects (Cambridge: Minor Planet Cent.)
Morbidelli, A., & Valsecchi, G. B. 1997, Icarus, 128, 464
Öpik, E. J. 1951, Proc. R. Irish Acad. A, 54, 165
Rauch, K. P., & Holman, M. 1999, AJ, 117, 1087
Saha, P., & Tremaine, S. 1992, AJ, 104, 1633
Shoemaker, E. M., & Wolfe, R. F. 1984, in Lunar and Planetary Science XV (Houston: Lunar Planet. Inst.), 780
Smith, B. A., et al. 1998, BAAS, 30, 1382
Smith, B. A., & Terrile, R. J. 1984, Science, 226, 1421
Stern, S. A., & Colwell, J. E. 1997, ApJ, 490, 879
Toomre, A. 1969, ApJ, 158, 899
Trilling, D. E., & Brown, R. H. 1998, Nature, 395, 775
Ward, W. R. 1981, Icarus, 47, 234
Weissman, P. R. 1996, in ASP Conf. Ser. 107, Completing the Inventory of the Solar System, ed. T. W. Rettig & J. M. Hahn (San Francisco: ASP), 265
Weissman, P. R., & Levison, H. F. 1997, ApJ, 488, L133
Wetherill, G. W. 1975, in Proc. 6th Lunar Sci. Conf., ed. R. B. Merrill (New York: Pergamon), 1539
Wisdom, J., & Holman, M. 1991, AJ, 102, 1528